Artur C. Bastos Neto, T.M.M. Ferron, Alain Chauvet, Farid Chemale,
Evandro F. de Lima, Luc Barbanson, Clovis F.M. Costa

U–Pb dating of the Madeira Suite and structural control of the albite-enriched granite at Pitinga (Amazonia, Brazil): Evolution of the A-type magmatism and implications for the genesis of the Madeira Sn–Ta–Nb (REE, cryolite) world-class deposit

- Artur C. Bastos Neto[a]
- José T.M.M. Ferron[b]
- Alain Chauvet[c]
- Farid Chemale Jr[d]
- Evandro F. de Lima[a]
- Luc Barbanson[e]
- Clovis F.M. Costa[b]

Highlights

Three successive episodes of A-type magmatism and basin formation occurred.
The albite-enriched granite emplacement occurred in a different tectonic setting.

Three types of structures concentrated the last magmatic-related fluid.
The data and interpretations imply crucial constraints on the petrologic models.

A comprehensive model for the geological evolution of the Pitinga region is proposed.

Abstract

The Madeira Sn–Nb–Ta deposit corresponds to the albite-enriched facies of Madeira granite (Madeira Suite) that is part of a NE–SW alignment of three granitic bodies. Structural analyses suggest that the albite-enriched granite emplacement and development of related structures occurred in a different tectonic setting than earlier facies of the granitic bodies in the NE–SW alignment and that the structure was dominated by a N-NE-trending shortening related to a left-lateral motion along a NE–SW corridor within a Riedel shear. Three types of structures (flat-lying, near vertical fractures, and geodes/miaroles) concentrated the last magmatic-related fluid in the albite-enriched granite. U–Pb in situ zircon dating of the albite-enriched granite yielded an age of 1822 ± 22 Ma. The other granitic plutons of the Madeira Suite, Água Boa granite (topaz-granite facies), and Europa per-alkaline granite formed at 1825 ± 14 Ma, 1831 ± 11 Ma, and 1839 ± 10 Ma, respectively. The granite bodies of the Madeira Suite occur in an area occupied by a cauldron complex composed of volcanic sequences (Iricoumé Group) and associated A-type granites (Mapuera Suite), and their formation was controlled by the reactivation of the cauldron structures and the pre-existing structures. The gap between the cauldron complex and the Madeira Suite is no greater than 35 Ma. The geological evolution was reanalyzed from the perspective of an entire extensional environment where three successive episodes of A-type magmatism and basin formation (Urupi Formation) occurred. The data and interpretations of this work imply crucial constraints on the petrologic models proposed for the albite-enriched granite and, consequently, on the genesis of the Madeira deposit.

Keywords

Pitinga;
Madeira deposit;
Albite-enriched granite;
A-type granite;
Paleoproterozoic

1. Introduction

The Pitinga Mine (Fig. 1) is the largest Sn producer in Brazil. The alluvial ore deposits, discovered in 1979 (Veiga et al., 1979), are almost exhausted. The Madeira deposit, discovered in 1983, is associated with albite-enriched granite (AEG)[1] facies of A-type Madeira granite (approximately 1820 Ma, part of the Madeira Suite). The Madeira deposit is a world-class deposit of 164 million tons of disseminated ore with a grade of 0.17% Sn (cassiterite). Niobium and Ta are exploited as byproducts. The potential byproducts of the disseminated ore are F (cryolite), Y, REE, Zr, Li, and Th. In addition, in the central portion of the Madeira deposit, there is a massive cryolite deposit of ten million tons with a grade of 31.9% cryolite (Na_3AlF_6). This association of rare metals in the same peralkaline rock that hosts a massive cryolite deposit is unique in the world.
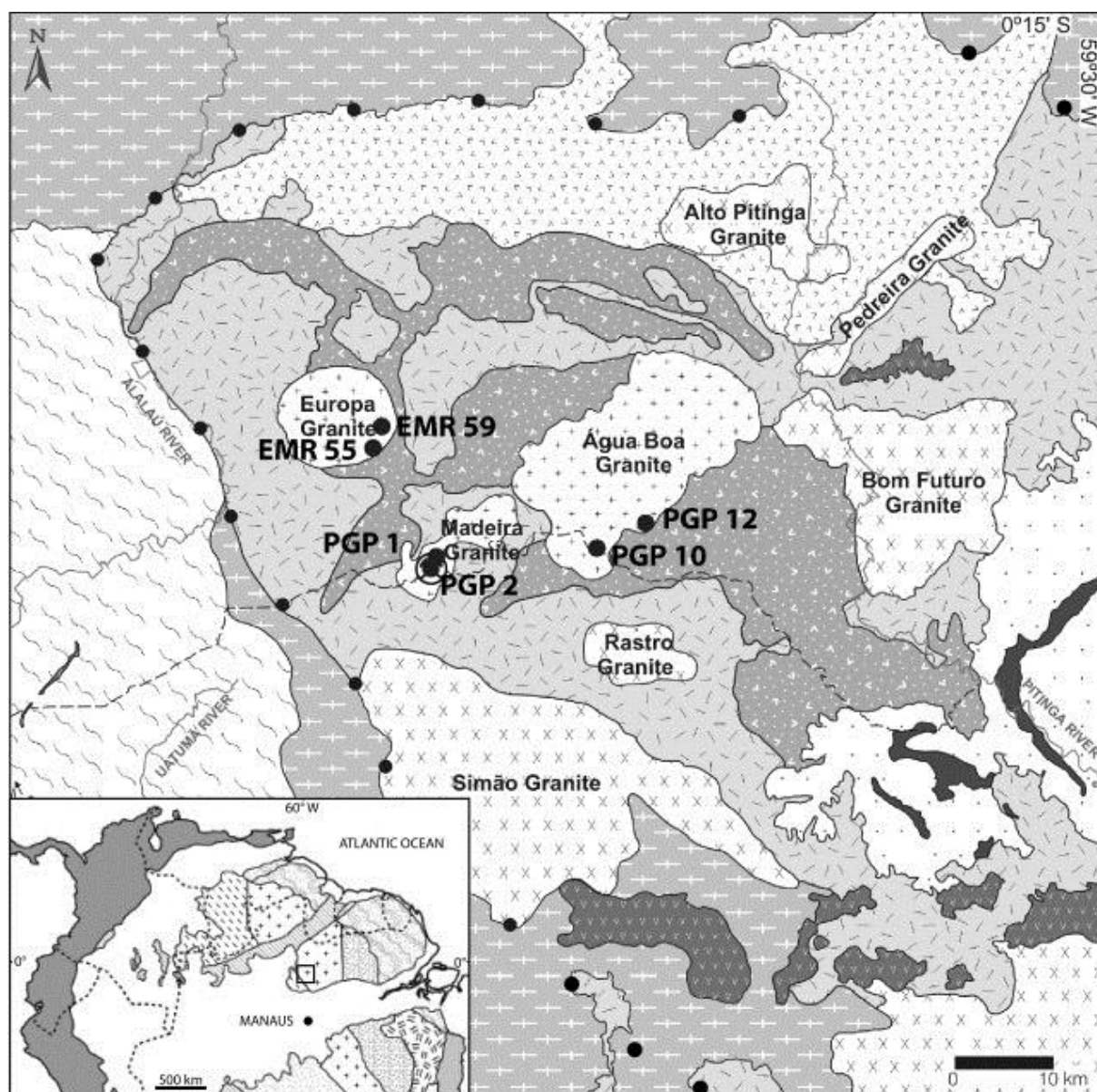
PROTEROZOIC	MESO		Seringa Formation	Alkaline basalt, diabase and gabbro
			Quarenta Ilhas Formation	Tholeiitic diabase, olivine diabase and differentiated acid rocks
	PALEO		Madeira Suite	Syenogranites and alkali-feldspar granite and leucogranite
		Uatumã Supergroup / Iricoumé Group	Urupi Formation	Quartz-arenite, arcoseous, siltite and interbedded pyroclastic with basal rocks of Paraiso Formation
			Mapuera Intrusive Suite	Syenogranite, monzogranite and leucogranite
			Ouro Preto Formation	Rhyolite, rhyodacite and quartz trachyte
			Paraiso Formation	Tuff and acid ignimbrite
			Divisor Formation	Porphyritic andesite and latite
			Água Branca Intrusive Suite	Monzogranite, biotite monzogranite, granodiorite, biotite granodiorite and tonalite
			Guianense Complex	Foliated granitoids, gneisses and mylonites

Legend:
- River
- Road
- Pitinga Mine

Fig. 1.

Geological map of the Pitinga mining district (after Ferron et al., 2010) and sample locations. The brachisyncline" of the Pitinga River is outlined by the Quarenta Ilhas Formation in the eastern part of the region. The volcanic rocks of the Iricoumé Group and the granites of the Mapuera Suite are bounded by an extensional megastructure (dotted line) that is approximately parallel to the brachisyncline. The insert is a map of the geological provinces of the Amazonia craton (Santos et al., 2000).

Bastos Neto et al. (2010) reviewed the geochemical and mineralogical characteristics of the Madeira deposit and the issues surrounding the crystallization of the AEG, such as the evolution of F fugacity in the magma, the magmatic-hydrothermal transition, and the massive cryolite deposit formation in the hydrothermal stage. Bastos Neto et al. presented a comprehensive evolutionary model. However, the origin of the magma that formed the AEG remains controversial, and results obtained from detailed petrological investigations allow for numerous interpretations. Alternative models, such as the two models presented by Lenharo (1998) and the two models presented by Costi (2000), have been proposed. Costi et al. (2010) also proposed a third petrological model based on the same geochemical data. Depending on the model, the AEG was either linked to the magma that formed the earlier metaluminous facies of the Madeira granite or the magma that formed other granitic rocks of the Pitinga region. All petrological models are perfectly plausible and consistent with the isotopic ages presented by the authors. However, no model is sustainable given the conflicting ages presented in the separate studies.

The Madeira granite body is elongated in a NE–SW direction (Fig. 1) and aligns with the Água Boa granite body (also of the Madeira Suite) and the Pedreira granite body (~1880 Ma, Mapuera Suite). Within the Água Boa granite, even the latest facies is elongated in a NE–SW direction. However, in the Madeira granite, the AEG, which is considered to be the most recent facies, has a N–S orientation. No studies have investigated whether the direction of the AEG emplacement indicates that it occurred in a tectonic setting different from that of the earlier facies. We consider this a very important issue that must be investigated and included in the discussion of the proposed models for the origin of the magma that formed the AEG.

Additional petrological studies are not required to determine the most compelling model to explain the generation of the AEG magma. Instead, the Madeira Suite needs to be dated and structural studies specifically focused on the relationship between the Madeira granite and AEG need to be included as support. The goal of this study is to discuss the AEG data with regard to the geological evolution of the Pitinga region that was revealed in recent regional studies carried out by our team. Using LAM-MC-ICP-MS, we present the first U–Pb ages in zircon obtained from the AEG and other rocks of the Madeira Suite. We also present preliminary, but significant, results from the first structural study performed on the AEG, which provide a valuable opportunity to study the structures and characteristics formed during the positioning and consolidation of a very uncommon magma.

2. Previous work

2.1. Geology of the Pitinga region

The Pitinga region (Fig. 1) is located in the southern portion of the Guyana Shield (Almeida et al., 1981), with older units grouped under the generic name of the Guyanese Complex (Issler et al., 1974). The Água Branca Suite (Araujo Neto and Moreira, 1976, Almeida et al., 1997) is composed of subduction-related calc-alkaline metaluminous granitoids (approximately 1950 Ma).

Mandetta et al. (1974) recognized the "brachisyncline" of the Pitinga River, which is outlined by the Quarenta Ilhas Formation in the eastern part of the region. According to Ferron et al. (2002) and Bastos Neto et al. (2005), the volcanic rocks of the Iricoumé Group (Veiga et al., 1979), which are part of the Uatumã Supergroup and the predominant unit of the Pitinga region, are bounded by an extensional megastructure (dotted line in Fig. 1) that is approximately parallel to the brachisyncline. The Paraiso Formation, which is part of the Iricoumé Group, outlines two semicircular structures that are joined close to the Europa granite. The Iricoume Group rocks, which have $^{207}Pb/^{206}Pb$ zircon ages between 1881 ± 2 and 1890 ± 2 Ma (Ferron et al., 2006), are mostly effusive and hypoabyssal rhyolites, highly welded ignimbrites, and ignimbritic tuffs, and they exhibit surge deposits. The alternating effusive and pyroclastic activities and the lack of evidence to support subaqueous deposits suggest that the environment was subaerial with cyclic effusive and explosive activities (Pierosan et al., 2011a and Pierosan et al., 2011b).

The granitic bodies located in the Mapuera Intrusive Suite (Araujo Neto and Moreira, 1976), part of the Uatumã Supergroup, intrude upon the Iricoumé Group. The granitic bodies have $^{207}Pb/^{206}Pb$ zircon ages between 1875 ± 3 Ma and 1888 ± 3 Ma (Ferron et al., 2006 and Ferron et al., 2010) and are arranged inside and along the border of the megastructure. These granitic bodies have varied forms, including subrounded (Rastro), irregular (Bom Futuro and Alto Pitinga), and elongated (Pedreira and Simão).

The volcanic (Iricoumé Group) and granitic (Mapuera Suite) rocks exhibit similar geochemical characteristics that can be attributed to their comagmatic character. These rocks range from metaluminous to slightly peraluminous and exhibit affinities for silica-saturated alkaline series and A-type magmas. They contain between 6.6 and 10.4% $Na_2O + K_2O$, 0.76 and 0.99% $FeO^t/(FeO^t + MgO)$, and 1.5 and 4.9% Ga/Al. The units plot in the intraplate or postcollisional fields in the Y + Nb vs. Rb diagram. The Nb/Y ratios indicate that these rocks are comparable to A2-type granites (Ferron et al., 2010).

In the megastructure, the substantial volume of pyroclastic rocks (especially rheoignimbrites) and effusive rocks (subordinate) with associated epizonal granitic bodies is similar to a caldera complex (Ferron et al., 2006). The contemporaneousness of volcanic units and granites, as shown by their Pb–Pb ages, suggests that these granites are the plutonic equivalents of volcanic rocks, a fact that is corroborated by their similar geochemical features. The association with the megastructure, which hosts the volcanic sequences, suggests that the positioning of these plutons was influenced or controlled by an extensional regime that led to the collapse of the caldera (Ferron et al., 2010, Pierosan et al., 2011a and Pierosan et al., 2011b).

The Urupi Formation consists of fluvial-eolian sandstones with pyroclastic interbeds (Veiga et al., 1979) that have a minimum age of 1780 Ma (Santos et al., 2002). Dated zircons from two cineritic tuff interbeds yielded Pb–Pb ages of 1882 ± 7.1 Ma and 1825 ± 3.9 Ma, respectively (Bastos Neto et al. unpublished results). The Madeira, Água Boa, and Europa granites (Fig. 1) are part of the Madeira Suite, have geochemical and mineralogical characteristics of A-type granites, and are described below. The Quarenta Ilhas Formation (zircon U–Pb age of 1780 ± 3 Ma) (Santos et al., 2002) includes tholeiitic basic rocks. Basic alkaline flows and dykes from the Mesoproterozoic (K/Ar from 1079 ± 18 Ma to 1090 ± 13 Ma, Araujo Neto and Moreira, 1976) are found together in the Seringa Formation (Veiga et al., 1979).

2.2. Madeira Suite and Madeira deposit

Europa peralkaline granite (Fig. 1) is gray and has a hypidiomorphic to equigranular coarse texture. The essential minerals are feldspar and quartz, the varietals are riebeckite and iron-richterite, the accessories are zircon and apatite, and the albite and biotite are products of hydrothermal alteration. Detailed descriptions are provided by Prado et al. (2007).

The Água Boa granite (Fig. 2) contains four facies. The older facies is a coarse-grained hornblende-biotite syenogranite, also known as rapakivi granite (Daoud and Antonietto, 1985), with associated Sn greisens (Borges, 2002 and Borges et al., 2009). The next two facies are a fine-grained porphyritic biotite syenogranite and a coarse- to medium-grained biotite-alkali-feldspar granite. The most recent facies is a topaz-bearing porphyritic biotite granite. Detailed descriptions are provided by Lenharo (1998).
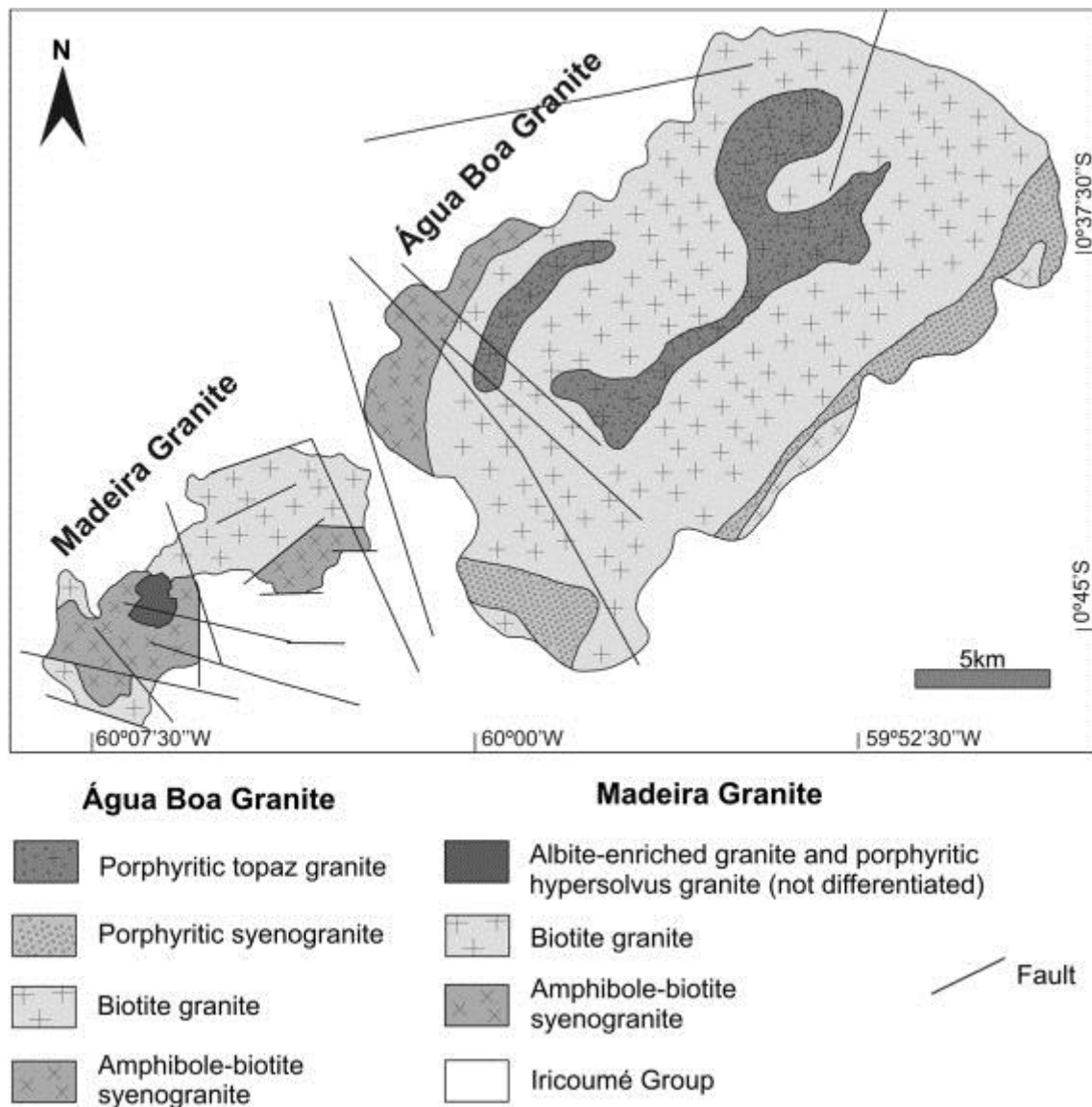
Fig. 2.

Geological map of the Madeira and Água Boa granites (Costi, 2000).

The Madeira granite contains four facies (Fig. 2 and Fig. 3). The amphibole-biotite syenogranite facies, also known as rapakivi granite, is equigranular to porphyritic and contains micrographic intergrowths in the porphyritic-type matrix biotite-amphibole symplectitic intergrowths, which suggests a shallow crystallization. The biotite-alkali-feldspar granite facies is peraluminous, equigranular, and locally porphyritic. The alkali feldspar hypersolvus porphyritic granite facies has phenocrysts (commonly substituted by chessboard albite) and a fine- to medium-grained matrix composed primarily of K-feldspar and quartz. According to Costi (2000), the hypersolvus granite and AEG interacted, were emplaced simultaneously, and intruded into the older facies.

Fig. 3. : Geological map of the albite-enriched granite (Minuzzi, 2005).

The AEG is subdivided into a core and a border. Disseminated ore occurs in both subfacies. The AEG core is subsolvus granite that is clear or dark gray, porphyritic to seriate in texture, fine to medium in grain s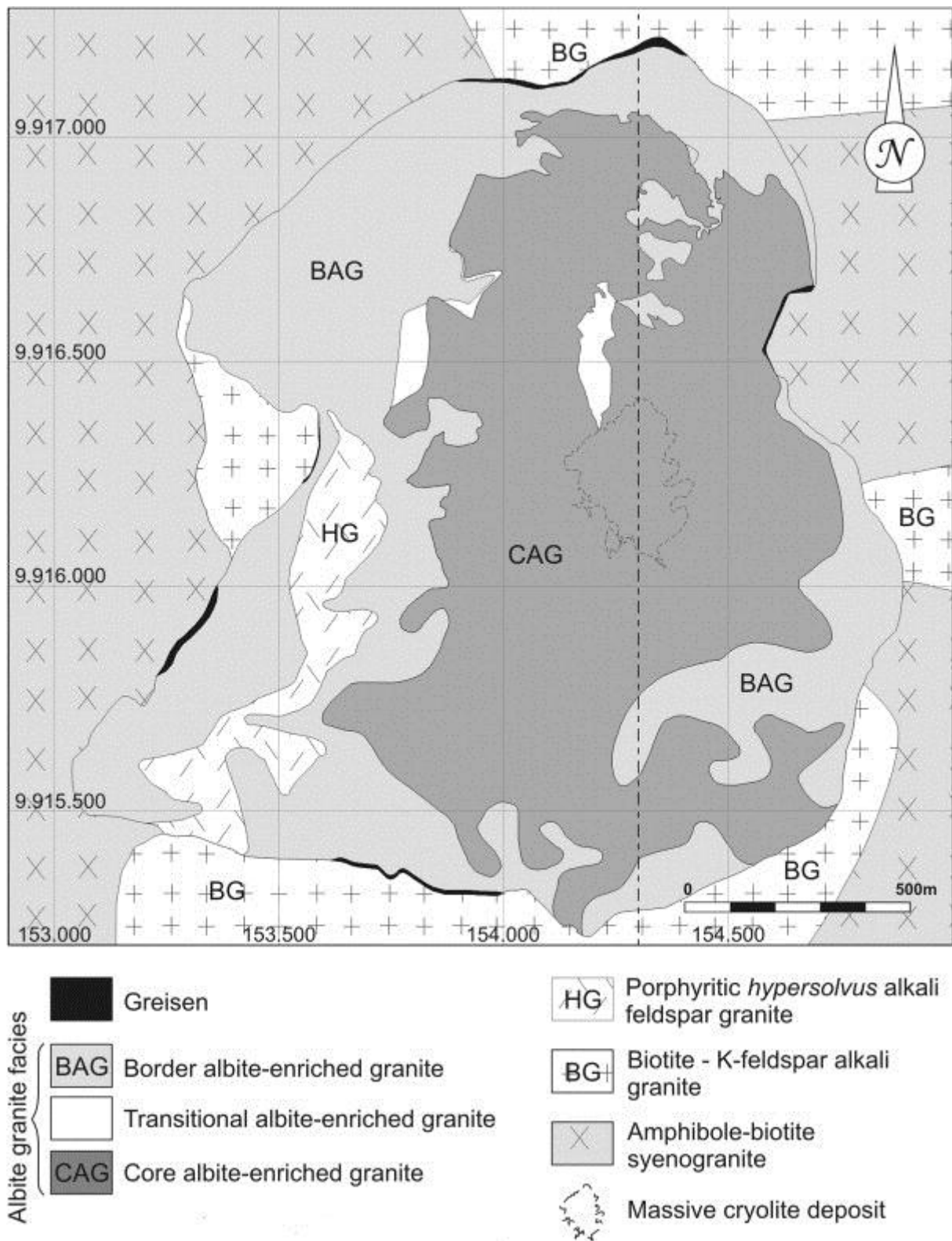ize, and composed primarily of quartz, albite, and K-feldspar in nearly equal proportions (25–30%). The accessory minerals are cryolite (5%), polylithionite (4%), green-brown mica (3%), zircon (2%), and riebeckite (2%). Pyrochlore, cassiterite, xenotime, columbite, thorite, magnetite, and galena are found in minor proportions. The AEG border is peraluminous granite that is dark red and presents the same texture types and essential mineralogy as the AEG core except for iron-rich minerals such as Fe–Li-mica, which have almost completely disappeared because of an autometasomatic process, and the presence of fluorite instead of cryolite (Costi, 2000). Detailed descriptions, including the composition of the ore minerals and potential by-products, are provided by Costi et al. (2010) and Bastos Neto et al., 2010 and Bastos Neto et al., 2012.

In the central portion of the Madeira deposit, there is a massive cryolite deposit of ten million tons with a grade of 31.9% cryolite (Na_3AlF_6). The massive cryolite deposit is formed by several massive bodies of cryolite that are intercalated with the AEG core and hypersolvus granite. These cryolite bodies are subhorizontal, can be up to 300 m long and 30 m thick, and are made up essentially of cryolite crystals (approximately 87% by volume) that can be up to 15 mm in diameter. The grains of quartz, zircon, and feldspar are generally <0.15 mm, homogeneously distributed, and account for approximately 13% by volume of the cryolite bodies. Detailed descriptions are provided by Bastos Neto et al., 2005 and Bastos Neto et al., 2010 and Minuzzi et al. (2006). The massive cryolite deposit was interpreted by Lenharo (1998) and Costi (2000) as being a magmatic deposit related to an extreme F-enrichment in the residual melt. However, according to Bastos Neto et al. (2010), the alleged extreme F-enrichment did not occur because the fugacity in the magma was buffered by the cryolite crystallization (disseminated cryolite in the AEG core), and the massive cryolite deposit is a hydrothermal deposit, as shown by the fluid inclusion data.

2.3. Controversies regarding the origin of the AEG magma and the age of the Madeira Suite

According to Lenharo (1998), all of the facies of the Madeira and Água Boa granites were formed from different mixtures of crustal and mantle sources, with prominent crustal contribution in all cases. Therefore, the AEG origin was either related to a specialized syenite or directly linked to the Europa peralkaline granite. According to Costi (2000), the AEG has either a mafic source with a short crustal residence time or a mantle source and was likely formed from a magma different from that which generated the earlier facies of the Madeira granite. Alternatively, Costi (2000) proposed that all of the facies of the Madeira granite came from the same magma and that the F-enrichment depolymerized the magma and reversed the crystallization trend from peraluminous with silica ascended to peralkaline with silica descended, thus forming the AEG. According to Costi et al. (2010), the F-rich peralkaline melt that produced the AEG was most likely the result of a phase-separation process, or immiscibility, similar to that described by Thomas et al. (2006) in which the peralkaline phase separated from a parental melt, most likely peralkaline to metaluminous that had a composition similar to that of the porphyritic hypersolvus alkali feldspar granite.

The ages calculated for the granitic bodies of the Madeira Suite (Table 1) are distributed over a relatively wide range; however, discrepancies reveal that there is still an important data gap. The supposed link between the AEG and Europa granite (Lenharo, 1998) would be untenable given the age of the latter body presented by Costi (2000). Using the same method, Lenharo (1998) calculated that the most recent facies (topaz granite) was older than the U–Pb age of

the rapakivi granite of the Água Boa. The models proposed by Costi (2000, second model) and Costi et al. (2010) rely on the Pb–Pb ages (Table 1) of the earlier facies and hypersolvus granite facies of the Madeira granite. The Pb–Pb ages are decreasing and very close, and the AEG was not successfully dated by this method. Nevertheless, these ages are much older than those obtained by Lenharo (1998) for the AEG. The U–Pb zircon age of the AEG obtained by Fuck et al. (1993) is also incompatible with the model that links the AEG with earlier facies of the Madeira granite.

Table 1.

Previous and this work geochronological data of the Madeira Suite.

	Age	Method	Author
Madeira granite			
Rapakivi granite facies	1824 ± 2 Ma	Pb–Pb Zr[a]	Costi et al. (2000)
Biotite granite facies	1822 ± 2 Ma	Pb–Pb Zr[a]	Costi et al. (2000)
Biotite granite facies	1810 ± 6 Ma	U–Pb Zr[c]	Lenharo (1998)
Hipersolvus granite facies	1818 ± 2 Ma	Pb–Pb Zr[a]	Costi et al. (2000)
Albite-enriched granite facies	1834 ± 6 Ma	U–Pb Zr[b]	Fuck et al. (1993)
Albite-enriched granite facies	1794 ± 19 Ma	U–Pb Zr[c]	Lenharo (1998)
Albite-enriched granite facies	1782 ± 4 Ma	Ar–Ar[d]	Lenharo (1998)
Albite-enriched granite facies	1822 ± 22 Ma	U–Pb[e] Zr	This paper
Água Boa granite			
Rapakivi granite facies	1798 ± 10 Ma	U–Pb Zr[e]	Lenharo (1998)
Biotite granite facies	1824 ± 24 Ma	U–Pb Zr[e]	This paper
Topaz granite facies	1815 ± 10 Ma	U–Pb Zr[c]	Lenharo (1998)
Topaz granite facies	1816 ± 20 Ma	U–Pb Zr[e]	This paper
Greisen	1783 ± 5 Ma	Ar–Ar[s]	Lenharo (1998)
Europa granite			
Europa alkali-feldspar granite	1829 ± 1 Ma	Pb–Pb Zr[a]	Costi et al. (2000)
Europa alkali-feldspar granite	1839 ± 6.2 Ma	U–Pb Zr[e]	This paper
Europa alkali-feldspar granite	1831 ± 11 Ma	U–PbZr[e]	This paper

a : $^{207}Pb/^{206}Pb$ zircon evaporation.
b : U–Pb zircon TIMS.
c : U–Pb zircon SHRIMP II.
d : Ar–Ar mica.
e : U–Pb zircon LA-MC-ICP-MS.

3. Methods

The structural study was performed in the open pit of the Madeira deposit where the AEG is exposed. We also described and measured some outcrops outside of the AEG (earlier facies of

the Madeira granite, Água Boa granite, and rocks of the Iricoumé Group) where the rocks are rarely exposed because of the Amazonian rainforest.

For the U–Pb zircon dating, six samples were collected (see locations in Fig. 1) from the following locations: (i) the core AEG (PGP-02) and border AEG (PGP-01) of the Madeira granitic body, (ii) the topaz facies (PGP-12) and biotite-granite facies (PGP-10) of the Água Boa granite, (iii) and two samples (EM-55, EM-59) of the Europa peralkaline granite from an Nb-anomalous zone.

The LA-ICP-MS analyses were carried out at the Federal University of Rio Grande do Sul (Brazil). All samples were mounted in epoxy in 2.5-cm-diameter circular grain mounts and polished until the zircons were just revealed. Images were obtained using an optical microscope (Leica MZ 125) and scanning electron microscope (Jeol JSM 5800). The zircon grains were dated with a New Wave UP213 laser (wavelength 213 nm) coupled to a ThermoFinnigan Neptune MC-ICP-MS. The repetition rate of the laser was 10 Hz. The energy varied from 0.3 to 1.1 mJ/pulse, and the corresponding spot sizes varied from 15 μm to 25 μm. The MC-ICP-MS was equipped with Faraday cups to measure the amount of ^{206}Pb, ^{208}Pb, ^{232}Th, and ^{238}U, and MIC channels were used to measure the amount of ^{202}Hg, ^{204}Hg+, ^{204}Pb, and ^{207}Pb. The main gas flow was 15 l/min, the auxiliary gas flow was 0.8 l/min, and the sample carrier gas flow was 0.8 l/min air + 0.45 l/min He. Data acquisition occurred in 50 cycles of 1.048 s integration time, and the masses 202, 204, 206, 207, 208, 232, and 238 were collected simultaneously. For every standard and sample set, blank values in the same conditions as the standard and sample were also measured. The average blank values were subtracted from all individual cycle measurements. The ^{204}Pb value was corrected for ^{204}Hg by assuming a ^{202}Hg/^{204}Hg ratio equal to 4.355. U/Pb ratios had an uncertainty of ±2% because of uncertainties in fractionation and mass spectrometry. In some instances, weak signals caused uncertainties to range up to ±4%. The values for the radiogenic ^{206}Pb, ^{232}Th, and ^{238}U that were collected by Faraday cups ranged up to 100 mV with less than 1% uncertainty. The ^{207}Pb mass was collected with a MIC channel, which can result in higher uncertainties, especially in samples with low amounts of radiogenic ^{207}Pb. Because common Pb causes greater uncertainty, we excluded cycles with f_{206} greater than 0.0025. The uncertainty introduced by laser-induced fractionation of elements and mass instrumental discrimination were corrected using a reference standard of zircon (GJ-1) (Jackson et al., 2004). The isotope ratios and inter-element fractionation of data obtained by the MC-ICP-MS instrument were evaluated by interspersing the GJ-1 zircon standard in every set of ten zircon samples (spots). The GJ-1 standard (GEMOC ARC National Key Center) meets the requirements for the methods used in our laboratory, and the ratios of ^{206}Pb*/^{238}U, ^{207}Pb*/^{206}Pb*, and ^{232}Th/^{238}U were homogeneous throughout the application of the "bracket" technique. External errors were calculated using error propagation of the individual measurements of the standard GJ-1 and measurements of the individual zircon samples (spots). Age was calculated using the program Isoplot 3.0 (Ludwig, 2003). Chemale et al. (2011) detailed the analytical methods and data treatment.

4. Results

4.1. Structural study of the albite-enriched granite

Three different types of structures were recognized in the AEG: geodes/miaroles, near-vertical fractures, and flat-lying structures.

(1)

Pneumatolytic features, or miaroles, occur as 10–50-cm geodes filled with variations of quartz, chlorite, fluorite, and cryolite. Along the eastern border of the AEG, both quartz-filled and quartz–fluorite-filled geodes were encountered (Fig. 4a and b). In some locations, the geodes aligned to form the initiation of the fractures (Fig. 4c). The intimate relation between the geode/miarole and the fracture is frequently observed. In the central portion of the AEG, this type of feature is also encountered in the form of relatively large spaces containing large growths of euhedral quartz, frequently associated with biotite (Fig. 4e and f). The preferred orientation of these large spaces remains difficult to ascertain because of their infrequency. The best expressions of geode/miarole features are found within the cryolite-rich zone, where several cm-scale quartz–cryolite and fluorite pockets were encountered.

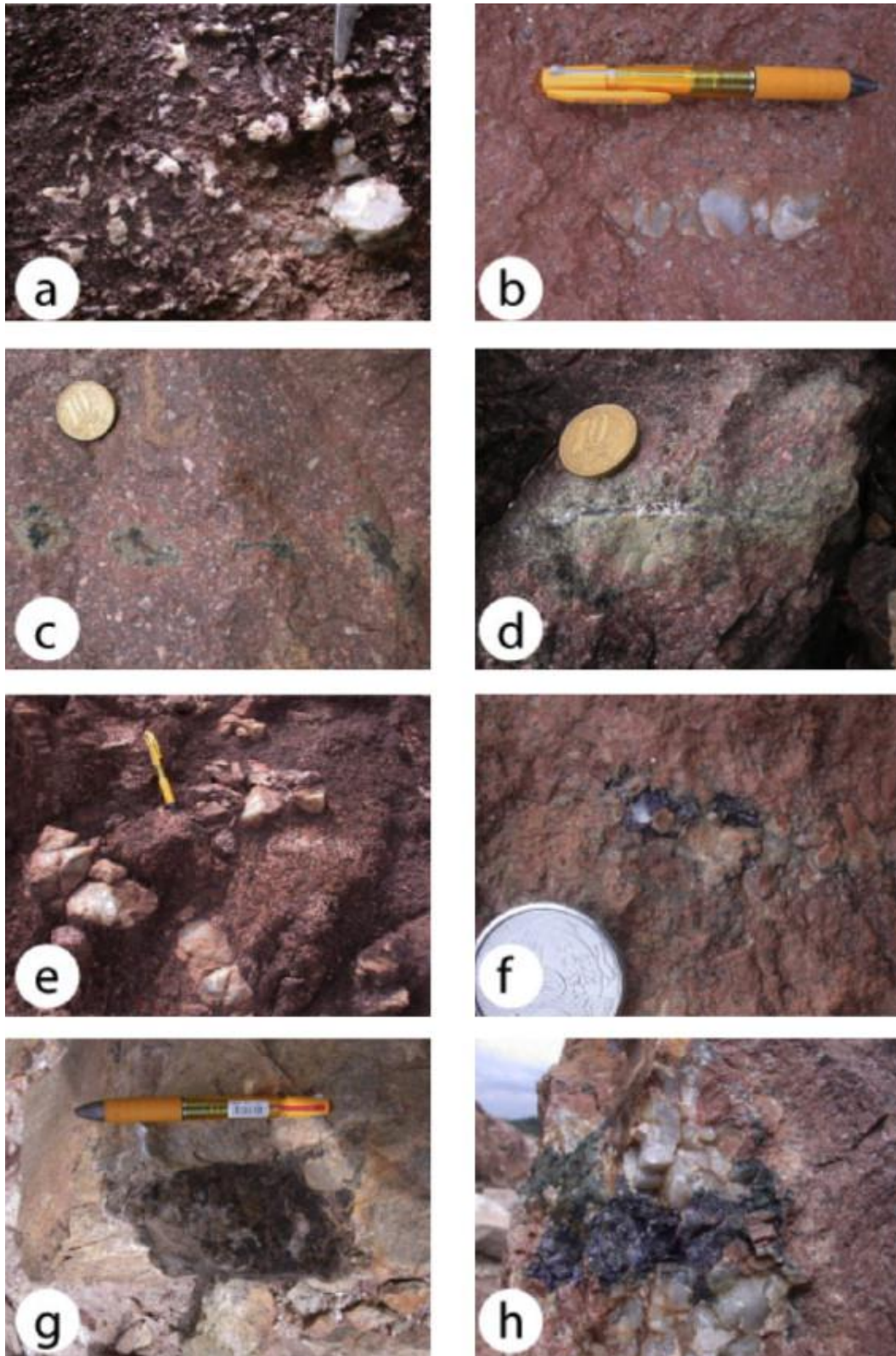Fig. 4. :Structures recognized in the albite-enriched granite. (A) Aligned quartz-filled geodes. (B) Aligned quartz–fluorite-filled geodes. (C) aligned geodes/miaroles forming the initiation of fractures. (D) Intimate relations between geodes/miaroles and the outlined fracture. (E) Geodes with euhedral quartz. (F) Aligned geodes with quartz and biotite. (G) Quartz–cryolite geodes/miaroles. H: quartz–cryolite–fluorite-filled geodes.

(2) Near-vertical fractures and dykes represent the major and most frequent structures of the studied area. The fractures were ubiquitous in the field, regardless of their geographic distribution within the albite granite or the variation in their content. Two types of fractures were identified: fractures filled by magmatic features, such as pegmatite and aplite, and thin fractures with or without filling. The pegmatite and aplite dykes were generally found within the AEG core. These dykes are most often vertical, with connected horizontal sills. Parallel to the pegmatite dykes, numerous quartz–cryolite geodes (Fig. 4g) and quartz–cryolite–fluorite geodes/miaroles (Fig. 4h) were encountered. The fractures are widespread throughout the AEG and occur as filled or unfilled structures. The filling is variable, with the most common composition being quartz, epidote, and kaolinite. Systematic measurement yielded two main directions of fracturing: N–S and E–W, with dominant N–S vertical-trending structures. The fracture distribution is arranged following an "en echelon" geometry consistent with a left-lateral large-scale motion (Fig. 5). The existence of the N–S-trending of large corridors of en echelon fractures can be observed at different scales and different points and must be taken into account when modeling the interaction between fracturing and pluton emplacement.
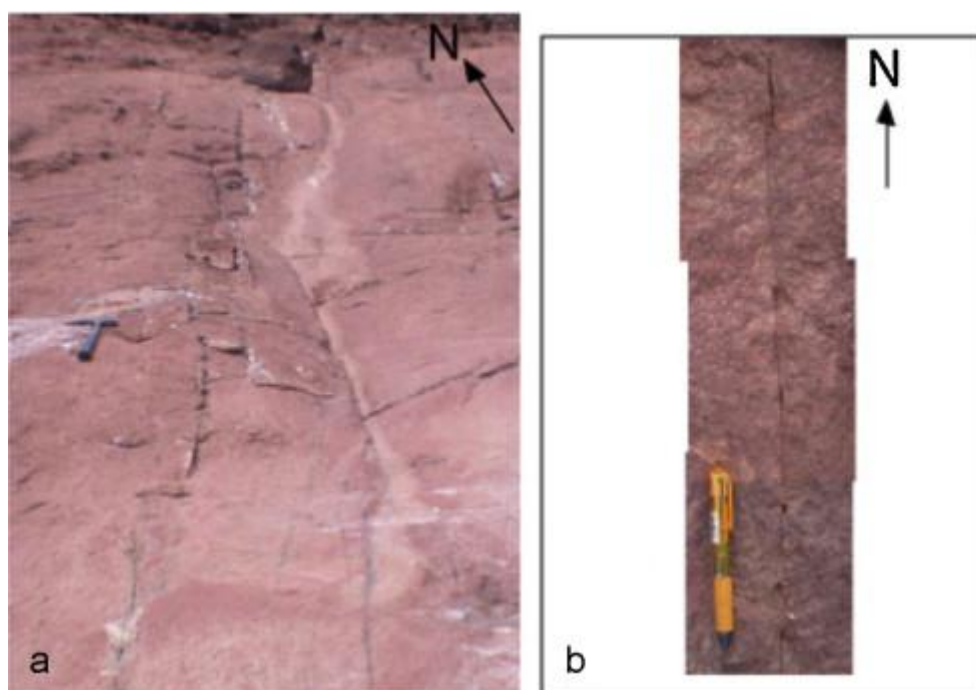
Fig. 5. : Two aspects of the geometry of en echelon and pull-apart fractures within the central part of the albite-enriched granite.

(3) Flat-lying structures are represented by flat cryolite–quartz pockets found in the vicinity of the pegmatite dykes and associated with the formation of magmatic sills. In addition to these structures, a few outcrops contain very thin, flat-lying planes filled with kaolinite. These planes appear as thin, white layers and are frequently associated with shear indicators. The kaolinite is secondary along these planes because of intense alteration processes. Because of parallelism with magmatic concentrations found in the AEG border, we suggest that these planes were magmatic in composition prior to the alteration.

Diagrams of all of the features measured in the field clearly indicate that N–S-trending structures are more frequent than NE-trending structures (Fig. 6). Detailed analysis reveals that the structures close to the N–S direction were mainly represented by thin, barren fractures and/or kaolinite-filled fractures and that the flat-lying features were systematically filled with kaolinite. We noted that the magmatic dykes (pegmatite and aplite) are parallel to the general direction of fracturing. At the map scale, the cryolite-bearing domain is located close to the center of the AEG core, whereas the borders are mainly characterized by the kaolinite-filled, near-vertical, and flat-lying fractures and veins. The fluorite–quartz miaroles are also concentrated close to the center of the AEG core.
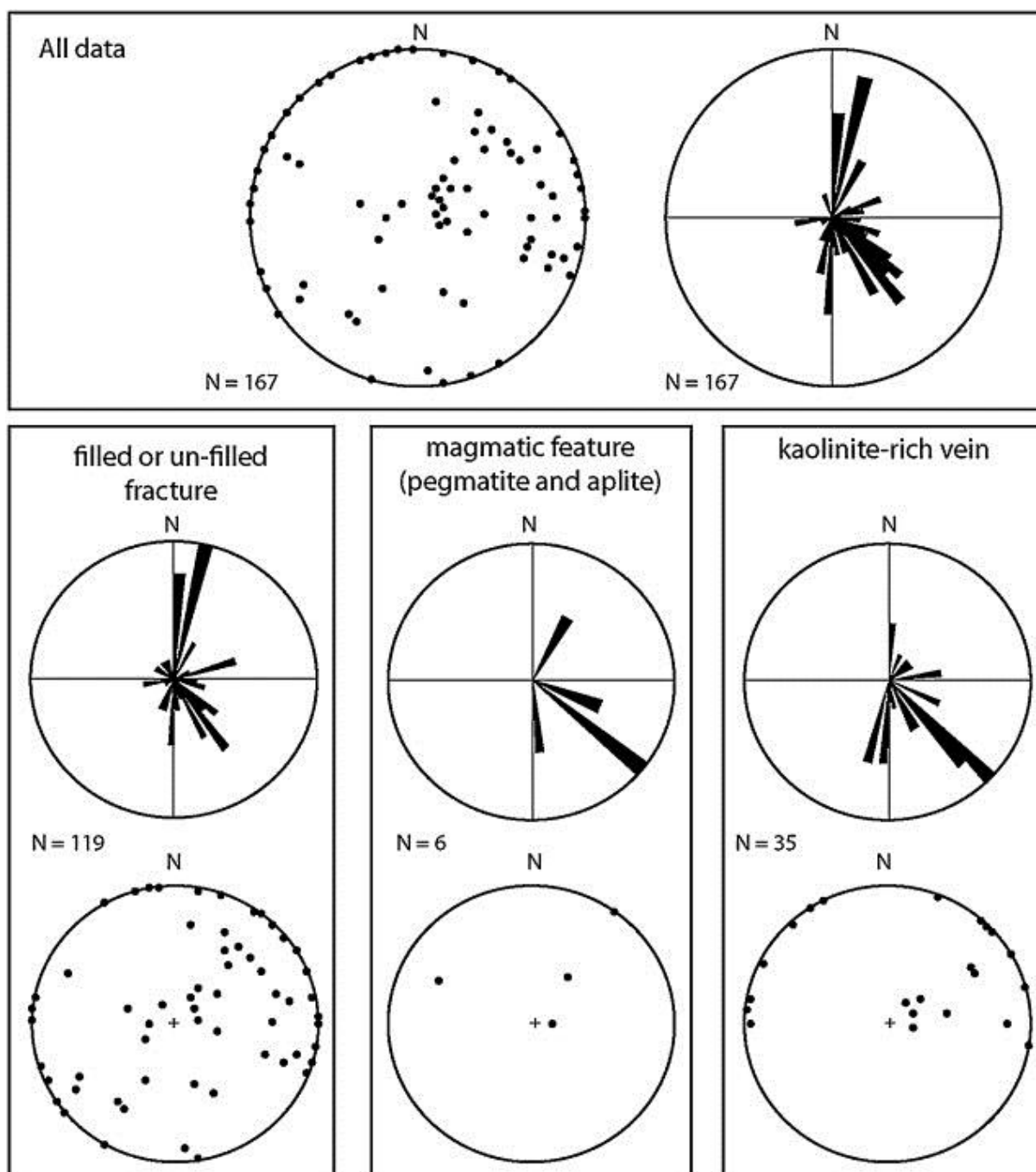
Diagrams are equal angle, lower hemisphere, Schmidt, stereonet.

Fig. 6. : Stereonet diagrams illustrating the orientation of all structures measured in the field.

4.2. Geochronology

The AEG (PGP-02) core sample was strongly altered by hydrothermal processes; the zircons have large amount of common Pb and inclusions. The U–Pb isotope data did not provide reliable age results due to the high amount of common ^{207}Pb and ^{206}Pb, which generally accounted for over 80% of the total Pb. Radiogenic Pb was found in very small amounts. Fig. 7A and B shows BSE images of separated zircons that have a patchy texture and large numbers of inclusions, which is indicative of strong alteration. According to the textural criteria in Corfu et al. (2003), these zircons show evidence of being strongly affected by late- to post-magmatic processes, as indicated by crystals with oscillatory zoning or growth partially preserved or obscured by recrystallization, which may be locally associated with the development of incipient convoluted zoning or well-developed in parts of the crystal. Crystals were also found with heterogeneous patchy patterns and convoluted zoning caused by the purification of the crystal structure after the crystallization, which is associated with the progressive migration of bands rich in trace elements. The mosaic patch texture, which indicates metasomatic replacement of a low-U domain by a U-rich domain (most likely associated with other trace elements), was incipiently developed, most frequently at the borders of certain crystals. These zircons were enriched with U and other trace elements, and their radiogenic Pb was replaced by common Pb because of metasomatic processes.
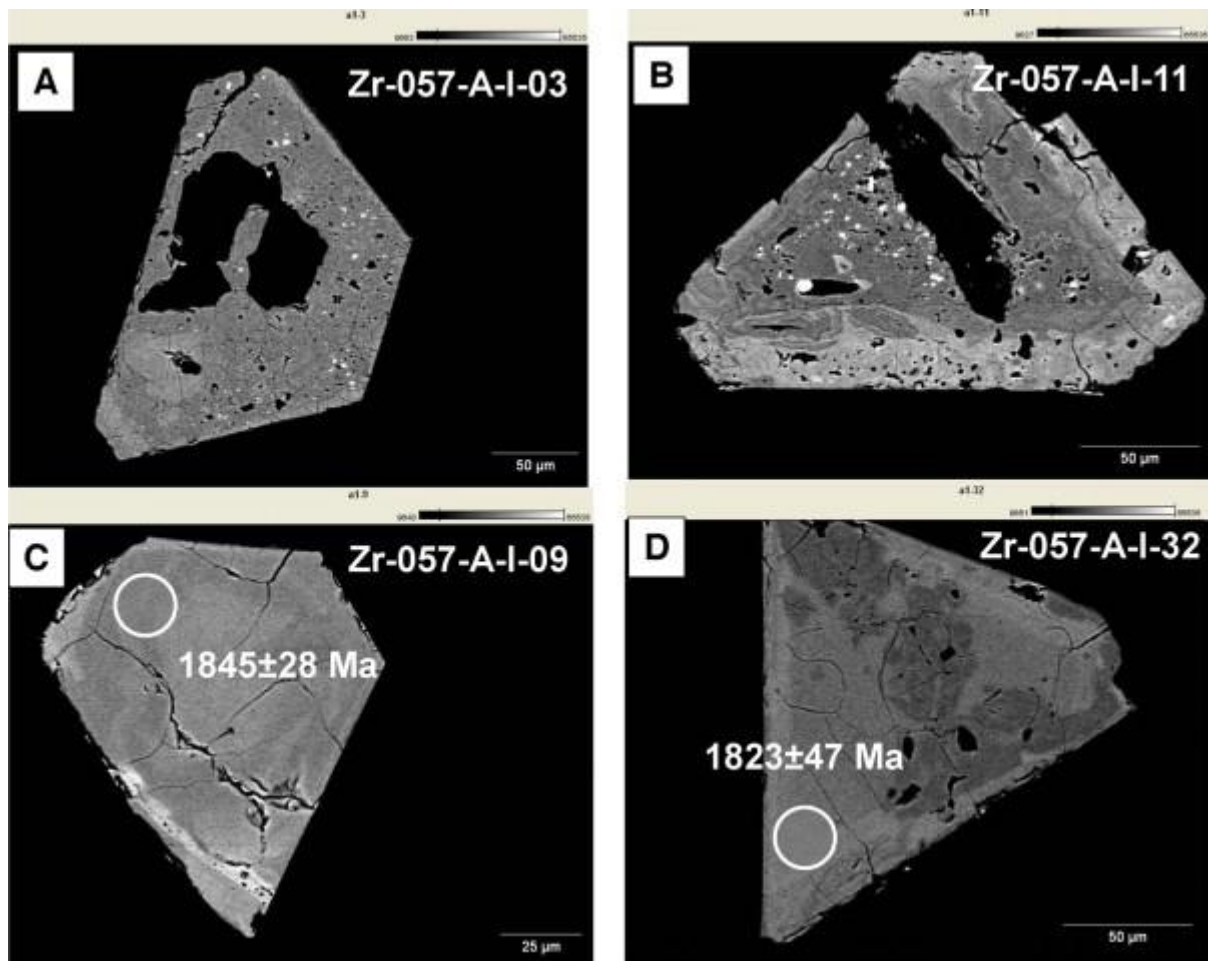
Fig. 7. : Back-scattering images from zircons of the albite-enriched granite. (A and B) Zircons from sample PGP-2, which were strongly affected by hydrothermal process (with high common Pb content and inclusions); a reliable U–Pb age was not obtained from these zircons because of common Pb in all parts of the zircons. (C and D) Dated zircons from sample PGP-1 (spot size 25 mm with $^{207}Pb/^{206}Pb$ age given in Ma), which were partially affected by later hydrothermal processes represented by fractures or dark areas (presence of common Pb). The sample PGP-01 from the AEG border contained totally altered zircon similar to that of the AEG core and partially altered zircon, as shown in Fig. 7C and D. The zircon crystals exhibit well-preserved phases and portions affected by fracturing, U-rich metasomatism, and radiogenic Pb replaced by large amounts of common Pb (see dark areas of Fig. 7D). Ten zircon grains were dated by LA-MC-ICPMS (sample PGP-01 in Table 2) and yielded an age of 1822 ± 22 Ma based on six concordant spots (Fig. 10).

Table 2.

Summary of LA-ICP-MS dating of the zircon grains from granitic samples from the Pitinga region.

Spot number	$^{206}Pb/^{204}Pb$	Th/U [a]	Isotope ratios[b]							Ages (Ma)						% Conc[e]
			$^{206}Pb/^{235}U$	1 s [%]	$^{206}Pb/^{238}U$	1 s [%]	Rho [c]	$^{207}Pb/^{206}Pb$ [d]	1 s [%]	$^{206}Pb/^{238}U$	1 s abs	$^{207}Pb/^{235}U$	1 s abs	$^{207}Pb/^{206}Pb$	1 s abs	
Sample PGP-01																
A-I-01	0.018	1.07	4.017	4.29	0.261	4.00	0.93	0.112	1.56	1494	60	1638	70	1827	28	82
A-I-09	0.008	0.48	4.584	2.01	0.301	1.15	0.57	0.110	1.64	1696	20	1746	35	1807	30	94
A-I-21	0.019	1.07	4.421	2.70	0.288	2.02	0.75	0.111	1.80	1630	33	1716	46	1823	33	89
A-I-31	0.002	1.17	4.621	1.29	0.300	0.93	0.72	0.112	0.90	1694	16	1753	23	1825	16	93
A-I-32	0.001	9.39	4.946	3.13	0.322	2.66	0.85	0.111	1.65	1798	48	1810	57	1824	30	99
A-I-25	0.023	6.15	2.253	3.31	0.147	2.32	0.70	0.111	2.36	883	21	1198	40	1821	43	48
A-I-04[f]	0.043	3.54	4.256	3.25	0.269	1.52	0.47	0.115	2.88	1535	23	1685	55	1877	54	82
A-I-06[f]	0.027	0.71	1.987	3.85	0.140	3.54	0.92	0.103	1.52	843	30	1111	43	1681	26	50
A-I-19[f]	0.033	1.86	2.179	4.90	0.149	3.97	0.81	0.106	2.86	898	36	1174	57	1727	49	52

Spot number	$^{206}Pb/^{204}Pb$	Th/U [a]	Isotope ratios [b]							$^{206}Pb/^{238}U$	1 s abs	$^{207}Pb/^{235}U$	1 s abs	$^{207}Pb/^{206}Pb$	1 s abs	% Conc [e]
			$^{206}Pb/^{235}U$	1 s [%]	$^{206}Pb/^{238}U$	1 s [%]	Rho [c]	$^{207}Pb/^{206}Pb$ [d]	1 s [%]							
A-I-26[f]	0.056	1.59	3.456	13.43	0.203	1.84	0.14	0.124	13.30	1191	22	1517	204	2008	267	59
Sample PGP-12																
C-III-01	0.008	0.52	3.456	3.29	0.229	2.42	0.74	0.109	2.23	1330	32	1517	50	1789	40	74
C-III-02	0.001	0.59	5.034	1.69	0.327	1.29	0.76	0.112	1.09	1824	23	1825	31	1826	20	100
C-III-05	0.002	0.54	3.492	3.53	0.233	2.71	0.77	0.109	2.26	1349	37	1525	54	1780	40	76
C-III-06	0.011	0.46	4.851	1.97	0.316	1.33	0.67	0.111	1.46	1771	23	1794	35	1820	27	97
C-III-07	0.000	0.47	4.877	1.31	0.318	0.88	0.67	0.111	0.97	1782	16	1798	24	1817	18	98
C-III-08	0.002	0.56	4.826	3.20	0.316	2.75	0.86	0.111	1.63	1772	49	1789	57	1810	30	98
C-III-09	0.005	1.07	4.482	2.32	0.296	1.55	0.67	0.110	1.72	1673	26	1728	40	1794	31	93
C-III-10	0.003	0.66	3.853	2.44	0.254	2.20	0.90	0.110	1.06	1459	32	1604	39	1799	19	81
C-III-11	0.001	0.38	4.838	1.88	0.317	1.33	0.71	0.111	1.32	1777	24	1791	34	1809	24	98
C-IV-04	0.003	0.71	4.828	2.75	0.321	1.86	0.68	0.109	2.03	1794	33	1790	49	1785	36	101

Spot number	$^{206}Pb/^{204}Pb$	Th/U[a]	Isotope ratios[b]							Ages (Ma)						% Conc[e]
			$^{206}Pb/^{235}U$	1 s [%]	$^{206}Pb/^{238}U$	1 s [%]	Rho[c]	$^{207}Pb/^{206}Pb$[d]	1 s [%]	$^{206}Pb/^{238}U$	1 s abs	$^{207}Pb/^{235}U$	1 s abs	$^{207}Pb/^{206}Pb$	1 s abs	
Sample PGP-10																
D-V-01	0.001	0.47	4.875	1.54	0.313	1.21	0.79	0.113	0.95	1755	21	1798	28	1848	18	95
D-V-05	0.001	0.39	4.872	1.18	0.313	0.64	0.55	0.113	0.99	1755	11	1797	21	1847	18	95
D-V-07	0.003	0.78	2.388	2.12	0.160	1.61	0.76	0.109	1.38	954	15	1239	26	1775	24	54
D-V-08	0.052	1.15	4.343	3.44	0.281	2.11	0.61	0.112	2.72	1595	34	1702	59	1836	50	87
D-V-11	0.003	0.42	4.869	1.38	0.315	0.92	0.67	0.112	1.03	1766	16	1797	25	1833	19	96
D-V-12	0.039	0.72	4.886	3.62	0.315	2.79	0.77	0.112	2.31	1766	49	1800	65	1839	42	96
D-VI-01	0.017	0.49	4.446	4.06	0.288	3.01	0.74	0.112	2.72	1630	49	1721	70	1834	50	89
D-VI-01 b	0.011	0.67	3.408	2.37	0.229	2.12	0.90	0.108	1.05	1330	28	1506	36	1763	19	75
D-VI-04	0.000	0.46	5.116	1.21	0.330	0.77	0.63	0.112	0.93	1839	14	1839	22	1839	17	100
D-VI-09	0.016	0.53	4.703	2.48	0.304	1.40	0.56	0.112	2.05	1709	24	1768	44	1838	38	93
Sample EMR-59																
E-VII-	0.001	0.35	5.103	1.99	0.330	1.1	0.58	0.112	1.62	1840	21	1837	37	1833	30	100

Spot number	206Pb/204Pb	Th/U [a]	Isotope ratios[b]							Ages (Ma)						% Conc [e]
			206Pb/235U	1 s [%]	206Pb/238U	1 s [%]	Rho [c]	207Pb/206Pb [d]	1 s [%]	206Pb/238U	1 s abs	207Pb/235U	1 s abs	207Pb/206Pb	1 s abs	
07							6									
E-VII-11	0.001	0.45	5.095	2.19	0.331	1.10	0.50	0.112	1.89	1842	20	1835	40	1828	35	101
E-VII-12	0.002	0.38	5.138	1.68	0.332	0.93	0.55	0.112	1.40	1846	17	1842	31	1838	26	100
E-VII-15	0.005	0.39	5.258	1.66	0.337	0.64	0.38	0.113	1.53	1870	12	1862	31	1853	28	101
E-VII-19	0.000	0.42	5.233	1.91	0.339	0.92	0.48	0.112	1.68	1880	17	1858	36	1834	31	102
E-VII-21	0.009	0.50	5.332	2.22	0.343	1.21	0.54	0.113	1.86	1903	23	1874	42	1841	34	103
E-VII-21 b	0.000	0.30	5.095	1.51	0.330	0.69	0.46	0.112	1.34	1839	13	1835	28	1832	24	100
E-VIII-01	0.001	0.68	5.373	2.09	0.347	1.16	0.55	0.112	1.74	1922	22	1881	39	1835	32	105
E-VIII-03	0.005	0.83	5.070	2.32	0.328	1.55	0.67	0.112	1.73	1830	28	1831	43	1832	32	100
E-VIII-08	0.004	0.52	5.235	3.46	0.324	2.04	0.59	0.117	2.80	1810	37	1858	64	1913	54	95
Sample EMR-55																
F-IX-02	0.001	0.48	5.202	2.52	0.331	1.58	0.63	0.114	1.96	1845	29	1853	47	1861	37	99
F-IX-03	0.002	0.45	5.130	2.36	0.329	1.3	0.56	0.113	1.95	1833	24	1841	44	1851	36	99

Spot number	$^{206}Pb/^{204}Pb$	Th/U [a]	Isotope ratios [b]							Ages (Ma)						% Conc [e]
			$^{206}Pb/^{235}U$	1 s [%]	$^{206}Pb/^{238}U$	1 s [%]	Rho [c]	$^{207}Pb/^{206}Pb$ [d]	1 s [%]	$^{206}Pb/^{238}U$	1 s abs	$^{207}Pb/^{235}U$	1 s abs	$^{207}Pb/^{206}Pb$	1 s abs	
F-IX-04	0.000	0.39	5.098	2.14	0.331	1.00	0.47	0.112	1.89	1845	18	1836	39	1825	35	101
F-IX-08f	0.020	0.78	5.321	1.84	0.343	0.65	0.36	0.113	1.72	1901	12	1872	34	1840	32	103
F-IX-11	0.003	0.41	5.134	1.42	0.330	0.87	0.61	0.113	1.13	1840	16	1842	26	1843	21	100
F-IX-15	0.000	0.39	5.294	1.32	0.345	0.49	0.37	0.111	1.22	1909	9	1868	25	1822	22	105
F-IX-16	0.026	0.49	5.052	1.87	0.327	1.01	0.54	0.112	1.58	1824	18	1828	34	1832	29	100
F-IX-18	0.000	0.48	4.987	1.57	0.325	0.83	0.53	0.111	1.33	1812	15	1817	29	1823	24	99
G-XI-01	0.002	0.45	5.080	2.84	0.327	1.21	0.42	0.113	2.57	1824	22	1833	52	1843	47	99
G-XI-02	0.006	0.47	5.070	2.23	0.327	0.95	0.42	0.113	2.01	1822	17	1831	41	1842	37	99

a

Th/U ratios are calculated relative to GJ-1 reference zircon.

b

Corrected for background and within-run Pb/U fractionation and normalized to reference zircon GJ-1 (ID-TIMS values/measured value); $^{207}Pb/^{235}U$ calculated using $(^{207}Pb/^{206}Pb)/(^{238}U/^{206}Pb * 1/137.88)$.

c

Rho is the error correlation defined as the quotient of the propagated errors of the $^{206}Pb/^{238}U$ and the $^{207}Pb/^{235}U$ ratio.

d

Corrected for mass-bias by normalizing to GJ-1 reference zircon and common Pb using the model Pb composition of Stacey and Kramers (1975).

e

Degree of concordance = (^{206}Pb/^{238}U age * 100/^{207}Pb/^{207}U age).

f

Not included in the age calculation.

The topaz granitic facies (PGP-12) and the biotite granite facies (PGP-10) of the Água Boa granite were both dated. Both granitic facies presented euhedral, long prismatic, clear igneous zircons and had similar Th/U ratios of between 0.38 and 1.15%. In Fig. 8A–D, the prismatic shape and age of the dated zircons can be observed. The dated zircons (Table 2) from the topaz-granite facies yielded a concordant age of 1816 ± 20 Ma (using the six most concordant zircons; Fig. 11A), whereas the biotite-granite facies yielded an age of 1824 ± 24 Ma (using all dated zircon grains and anchored at their origin; Fig. 11B). The zircon crystals in both samples from the Europa granite are well crystallized, euhedral, and contain rare mineral inclusions (Fig. 9A–D). The results from sample EM-59 (Fig. 11C) indicate a concordant age of 1839 ± 6.2 Ma with a Th/U ratio of between 0.30 and 0.83% (Table 2). Nine out of ten zircons from the EM-55 sample yielded a concordant age of 1831 ± 11 Ma (Fig. 11D), with a Th/U ratio of between 0.39 and 0.78%.
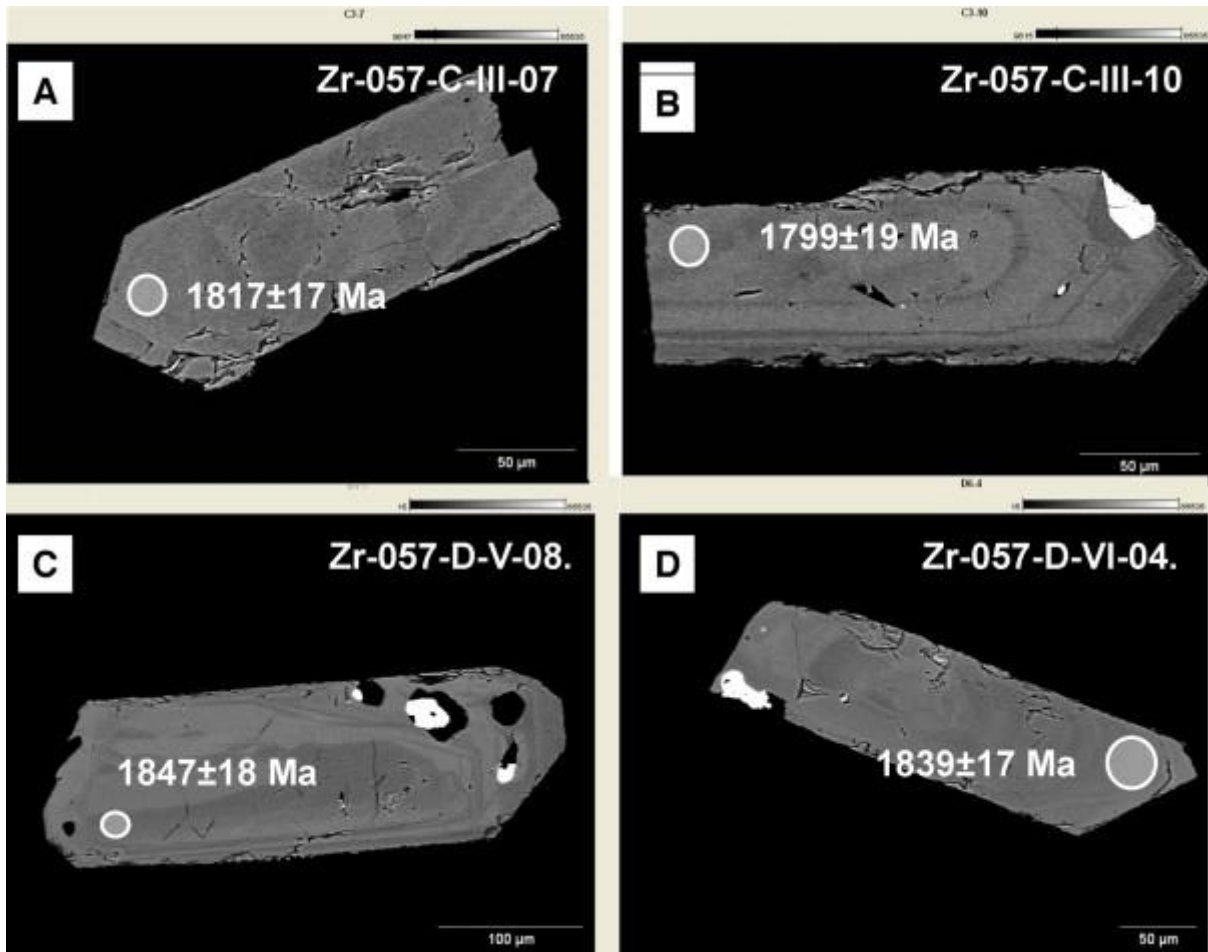

Fig. 8. : Back-scattering images from zircons of the Agua Boa granite including $^{207}Pb/^{206}Pb$ age and respective laser spot (diam. = 25 mm). (A and B) Sample PGP-12. (C and D) Sample PGP-10.
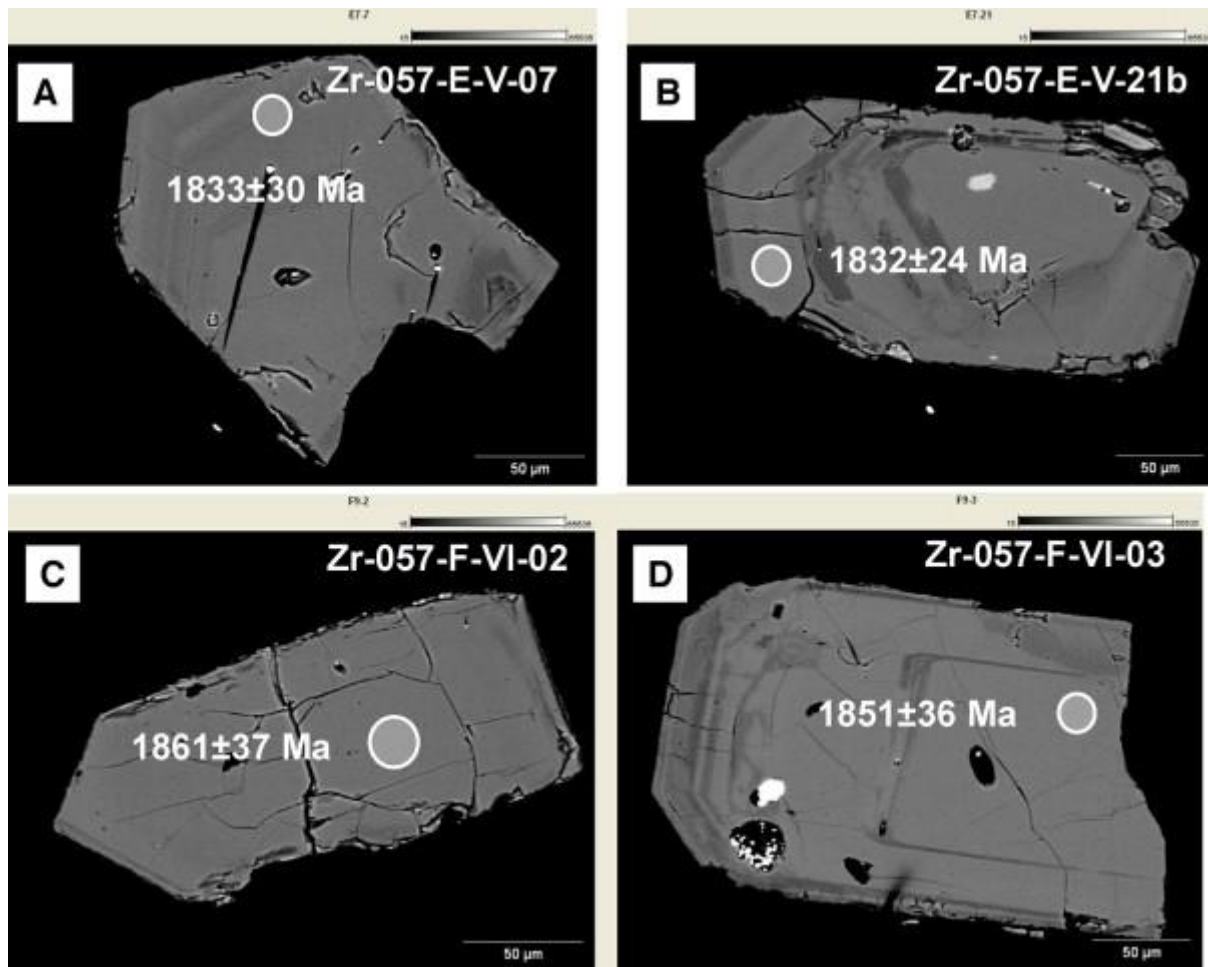
Fig. 9. : Back-scattering images from zircons of the Europa granite with $^{207}Pb/^{206}Pb$ age and respective laser spot (diam. = 25 mm). (A and B) Sample EMR-55. (C and D) Sample EMR-59.

5. Discussion

5.1. Albite-enriched granite emplacement

In the AEG emplacement, several outcrops indicate a direct relationship between magmatic and hydrothermal features. A spatial association exists between miaroles and fractures, with miaroles and geodes appearing to be the earliest structures, followed by the formation of fractures. All of the intermediate stages were observed, including isolated miaroles, aligned miaroles, aligned miaroles overprinted by a fracture, and clearly formed fractures. This sequence of formation is consistent with the mineralogical constraints of the AEG. The pneumatolytic stages, such as fluorite and cryolite, are mainly found within the geodes and miaroles or as the disseminated phase within the granite. Inversely, the presence of these minerals within the fractures is rare, with the fractures essentially filled with quartz and kaolinite, which is to be expected given that kaolinites are representative of ancient aplite sills and dykes. The initial stages are characteristic of pneumatolytic conditions, and the later stages exhibit hydrothermal features.

The AEG emplacement and the development of its structures were continuously controlled by a tectonic setting dominated by a N-NE-trending shortening. The combination of this tectonic

setting and late magmatic stages explains why we found three types of structures: (i) flat-lying structures, (ii) near-vertical fractures, and (iii) geodes/miaroles. The existence of specific structural geometries, such as pull-apart and en echelon fractures, confirm the constant tectonic control. The structures created during this tectonic-controlled emplacement concentrated the last magmatic-related fluid. Pegmatite sills and dykes, miaroles, and numerous aplite sills and dykes were formed and filled during the initial stages. The cooling of the granite and ongoing deformation allowed the formation of fractures with a specific geometry acquired in response to the N-NE-trending shortening. All of the vertical fractures with pull-apart geometry are consistent with this tectonic setting. We suggest that the formation of the en echelon fractures resulted from a left-lateral motion along the NE–SW corridor, in the position of Riedel shear (Fig. 12).
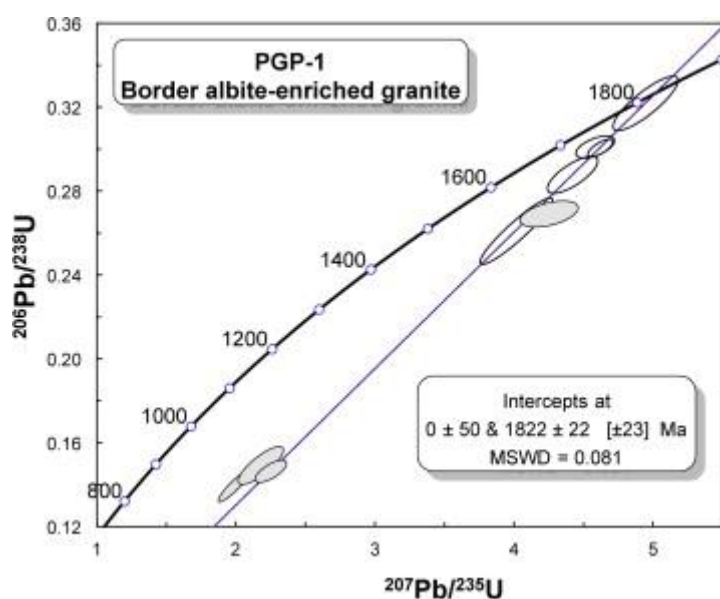

Fig. 10. : Concordia diagram for the Madeira granite albite-enriched facies border (sample PGP-1). Gray ellipses are not included in the age calculation.
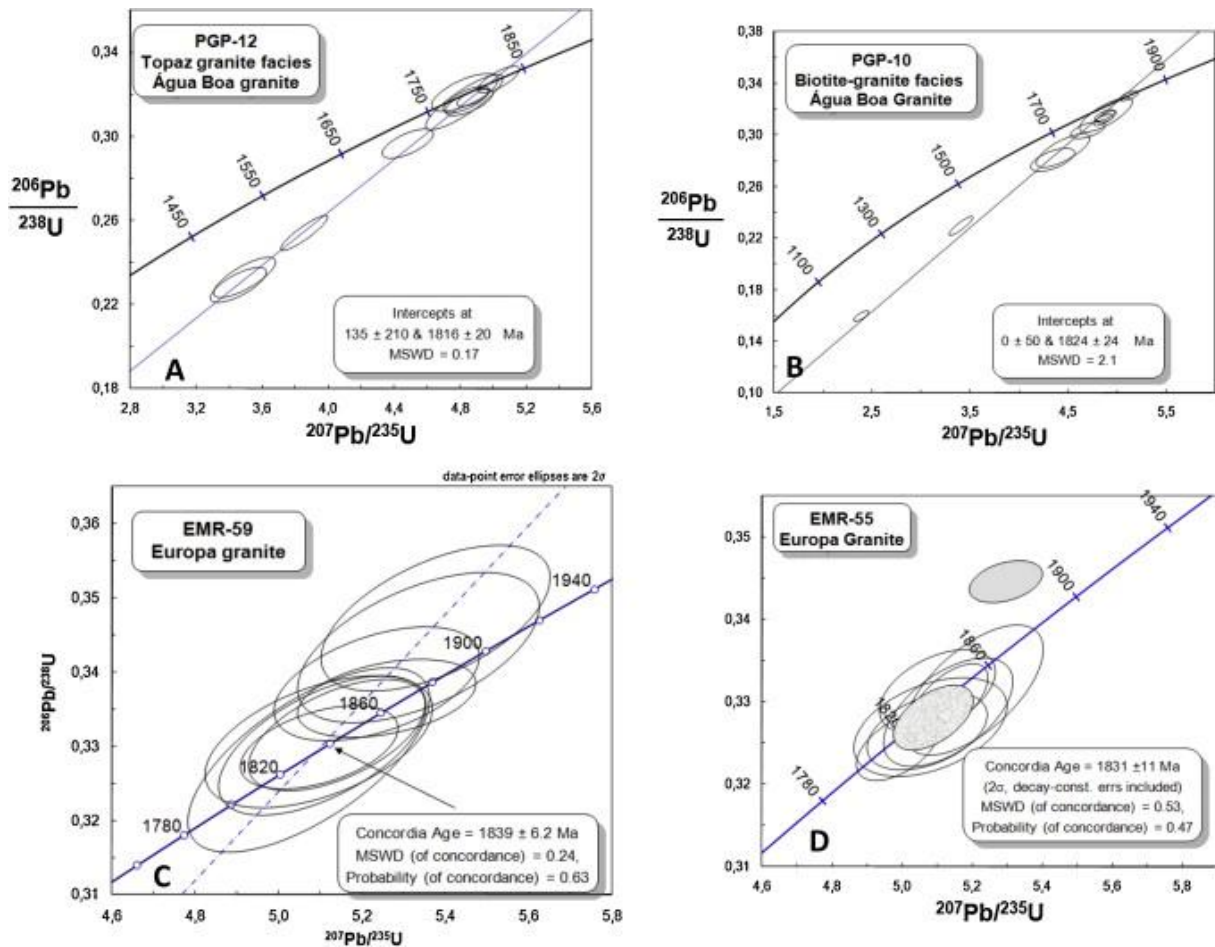
Fig. 11. : Concordia diagrams for different granites of the Pitinga district. (A) Água Boa granite, sample PGP-12 (topaz granite facies), with a concordant age of 1816 ± 20 Ma. (B) Água Boa granite, sample PGP-10 (biotite granite facies), with a concordant age of 1824 ± 24 Ma. (C) Europa granite, sample EMR-59, with a concordant age of 1839 ± 6.2. (D) Europa granite, sample EMR-55, with a concordant age of 1831 ± 11 Ma.
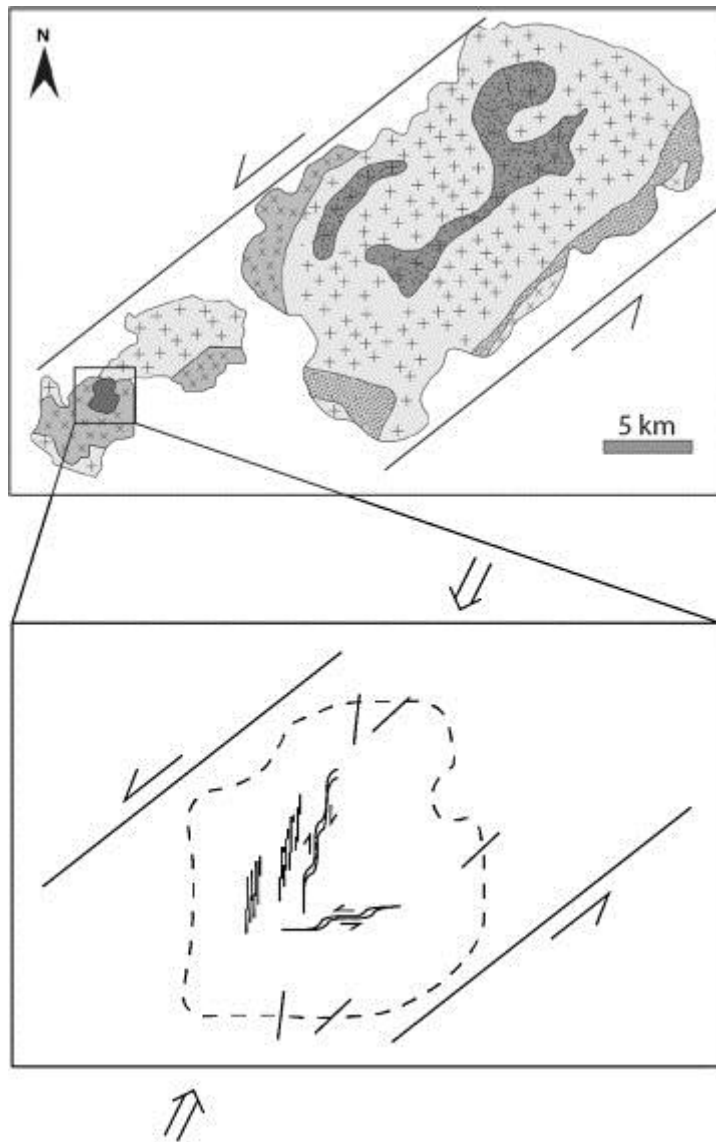
Fig. 12. : Simplified geological map and structural sketch of the magmatic intrusion of albite-enriched granite controlled by left-lateral motion along the NE–SW-trending lineament. See text for explanation.

The formation of flat-lying veins that mainly trend NS and NE–SW, record E-directed reverse motions, and are concentrated along the AEG borders has not yet been explained. Two alternative modes of formation can be suggested. The first alternative is that the vertical and flat-lying structures were created by the combined effects of the main ($\sigma1$) and intermediate ($\sigma2$) constraints. These two constraints have similar values; thus, the co-formation of the strike-slip and tangential structures during the late evolution of the AEG is possible. The second alternative is that the flat-lying structures were created by pluton-related forces and are not correlated with regional tectonics.

We suggest herein a model of AEG emplacement dominated by a N-NE-trending shortening related to a left-lateral motion along a NE–SW corridor, in the position of Riedel shear. Thus, the orientation of the AEG, elongated in the N–S direction, is not casual. This corridor was active because of the Pedreira granite (Mapuera Suite, approximately 1880 Ma) (Fig. 2)

emplacement and it also controlled the Água Boa granite and the Madeira granite early facies (~1830 Ma). However, the striking NE–SW orientation of all these rocks clearly results from different prevailing tectonic regime. The existence of a substantial time lag between the emplacement of the early facies of the Madeira granite and the AEG may provide evidence that the AEG localization within the Madeira granite is casual and that a link with the earlier facies of the Madeira granite is unlikely.

5.2. Madeira Suite magmatism age

Based on U–Pb in situ zircon dating by MC-ICPMS, the Europa granite body formed between 1831 ± 11 and 1839 ± 6.2 Ma. The age obtained by $^{206}Pb/^{207}Pb$ dating for the same granitic body is 1829 ± 1 Ma, as published by Costi et al. (2000), and is in agreement with our data. It follows that the Europa granite was the first pluton of the Madeira Suite to be positioned.

The ages obtained by U–Pb in situ zircon dating for the topaz granite facies (1816 ± 20 Ma) and biotite granite facies (1824 ± 24 Ma) of the Água Boa granite body are consistent with a contact relationship between these facies. Lenharo (1998) obtained a U–Pb age of 1798 ± 10 Ma in the rapakivi granite (earlier facies) and 1815 ± 10 Ma in the topaz granite (later facies) and interpreted that the age of the topaz granite, whose melt would have incorporated the zircons from the host rocks, was incorrect. Our results indicate that age of the rapakivi granite, whose age is presumed to be somewhat older than what we obtained for the biotite granite facies, was incorrect.

Zircons from the AEG contain evidence of being strongly affected by late- to post-magmatic processes that complicate precise dating. The U–Pb in situ LA-MC-ICP-MS age is 1822 ± 25 Ma, which we interpret as the igneous age of the magmatic phase. Considering the margin of error, this age is compatible with the U–Pb ages of 1834 ± 6 Ma (Fuck et al., 1993) and 1794 ± 19 Ma (Lenharo, 1998). Taking into account the structural data and the U–Pb ages, the age of this body is between 1794 ± 19 Ma and 1822 ± 22 Ma. It is important to note that Ar–Ar isotopes are very sensitive to metasomatic/hydrothermal processes; thus, the Ar–Ar in mineral (micas) published by Lenharo (1998) for the Água Boa granite body (1783 ± 5 Ma) and Madeira granite body (1782 ± 4 Ma) correspond to an important metasomatic/hydrothermal event.

5.3. Geological evolution of the Pitinga region and implications for the AEG models

In light of the available data from the 1990s and taking into account the age of the Iricoumé Group ($1962+42/-33$ Ma) (Schobbenhaus et al., 1994) and the Madeira Suite (Table 1), the age gap between the Iricoumé Group and Madeira Suite was approximately 130–170 Ma. Data on the granitic bodies of the Mapuera Suite were lacking. In all the studies, the rocks of the Iricoumé Group were briefly described, and a connection between these rocks and the granitic bodies of the Madeira Suite was not suspected.

Given current information, the gap between the cauldron complex (Iricoumé Group with associated granitic bodies of the Mapuera Suite) and the Madeira Suite is approximately 35 Ma, and was considered with the ages of the Simão granite (1875 ± 4 Ma; Ferron et al., 2006) and the Europa granite (1839 ± 10 Ma; the present work). Considering the margins of error, the gap would only be 22 Ma. Moreover, Mapuera plutons that have not yet been dated might indicate an even younger age.

The granite bodies of the Madeira Suite only occur in the area occupied by the volcanic sequences. Their shapes are similar to those of the Mapuera granitic bodies; thus, their emplacement was likely controlled by the reactivation of the cauldron complex structures and pre-existing structures, such as the NE–SW corridor that previously controlled the positioning of the Pedreira granite (Mapuera Suite). Therefore, the spatial and temporal relationships between the magmatism of the Iricoumé-Mapuera and that of the Madeira Suite are much narrower than previously suggested. Consequently, the geological evolution of the Pitinga region, from the Iricoumé Group until the AEG, must be reanalyzed from an extensional environmental perspective in which the basin formation (Urupi Formation) and three successive episodes of A-type magmatism occurred.

The first episode of A-type magmatism (Iricoumé Group and Mapuera Suite) resulted from mantle sources previously modified by subduction (Ferron et al., 2006 and Ferron et al., 2010). In the second episode, numerous distinctive magmas (Europa granite, Água Boa granite, and the early facies of the Madeira granite) formed from different mixtures of crustal and mantle sources (Lenharo, 1998). The third stage, represented by the AEG, evolved from a change in the tectonic setting. For the third stage, the richness in Sn indicates a much more substantial participation of crustal components in the melt generation.

The data and interpretations contained in this work imply crucial constraints on the petrologic models proposed for the AEG. (1) The structural data refute the model by Costi (2000) that links the origin of the AEG with the same magma that formed the earlier facies of the Madeira granite. (2) The ages obtained for the Europa granite show that this body is not comagmatic with the AEG, which means that the AEG cannot be related to the Europa granite (Lenharo, 1998) by fractional crystallization or other differentiation processes. (3) The geological evolution, characterized by three successive stages of A-type magmatism from sources successively more shallow, refutes the model that links the AEG to a mantle source (Costi, 2000, first model). The only petrologic model that cannot be ruled out by our current study is that of Costi et al. (2010).

The model created by Martin (2006), which relates the A-type granites of crustal origin to the open-system fenitization-type reactions controlled by alkali- and silica-bearing mantle-derived fluid in an extensional environment, accommodates all of the features described above as long as a gradual rise of isotherms along the successive tectonic reactivations is taken into account. The generation of the AEG melt would be related to a step of the isotherm rise assigned to the tectonic reactivation that controlled the AEG emplacement, which occurred when mantle fluid ascended further into the crust, promoted fenitization-type reactions in rocks previously enriched in Sn, and introduced elements such as F, Nb, Y, REE, and Th in anomalous concentrations. It is possible that these rocks were already being fenitized in the previous stage and that the third stage allowed for the input of an F-rich fluid that generated metasomatism, causing the differential for the rock to become fusible and form the AEG melt.

6. Conclusions

The Europa granite, dated at 1831 ± 11 and 1839 ± 6.2 Ma, was the first pluton of the Madeira Suite to be positioned. We obtained the first ages for the Água Boa granite that were consistent with a contact relationship between the facies within the body (1824 ± 24 Ma in the biotite granite facies and 1816 ± 20 Ma in the topaz granite facies). These ages indicate that this pluton is approximately synchronous with the early facies of the Madeira granite. The

AEG was crystallized between 1822 ± 22 Ma and 1794 ± 19 Ma, with strongly hydrothermal process occurring at 1782 ± 4 Ma (Lenharo, 1998). The AEG emplacement and the elongated shape in a N–S direction are related to a tectonic setting different from what occurred during the emplacement of the Água Boa granite and earlier facies of the Madeira granite. The emplacement and development of the structures in the AEG were continuously controlled by a tectonic setting dominated by a N-NE-trending shortening related to a left-lateral motion along a NE–SW corridor. The combination of this tectonic setting and late magmatic stages created three types of structures (flat-lying structures, near vertical fractures, and geodes/miaroles) that concentrated the last magmatic-related fluid. The presence of pull-apart and en echelon fractures confirm the constant tectonic control.

The spatial and temporal relationships between the Madeira Suite and the cauldron complex, formed by the Iricoumé Group and the associated granites of the Mapuera Suite, are much narrower than previously suspected, with a gap of approximately 30 Ma. The emplacement of the granite bodies of the Madeira Suite was controlled by the reactivation of the cauldron complex structures and pre-existing structures. Consequently, the geological evolution from the Iricoumé Group to the AEG was analyzed considering the entire extensional environment in which the basin formation and three successive episodes of A-type magmatism occurred.

The data and interpretations contained in this work imply crucial constraints on the petrologic models proposed for the AEG. The structural data refute models that link the origin of the AEG with earlier facies of the Madeira granite. Age analysis makes it impossible to relate the AEG to the Europa granite by fractional crystallization or other differentiation processes. The geological evolution, characterized by three successive stages of A-type magmatism from increasingly shallow sources, refutes the model that links the AEG to a mantle source. Taking into account the geological evolution of the region, we conclude that the model described by Martin (2006) for A-type granites accommodates all of the features found in the Pitinga region. We propose that the generation of the AEG melt was related to a third step of the isotherm rise in an extensional environment in which mantle fluid ascended further into the crust, promoted fenitization-type reactions in rocks previously enriched in Sn, and introduced elements such as F, Nb, Y, REE, and Th in anomalous concentrations.

Acknowledgements

References

F.F.M. Almeida, Y. Hasui, B.B. Brito Neves, R.A. Fuck
Brazilian structural Provinces: an introduction
Earth-Sciences Reviews, 17 (1981), pp. 1–29

M.E. Almeida, L.M.B. Fraga, M.J.B. Macambira
New geochronological data of calci-alkaline granitoids of Roraima State, Brazil
South-American Symposium on Isotope Geology, Campos do Jordão (1997), pp. 34–37

H. Araujo Neto, H.L. Moreira
Projeto Estanho de Abonari
Companhia de Pesquisa de Recursos Minerais, Manaus (1976) (unpublished report)

A.C. Bastos Neto, V.P. Pereira, E.F. Lima, J.M.T.M. Ferron, O.R.R. Minuzzi, M. Prado, L.H. Ronchi, J.C. Frantz, N.F. Botelho
O depósito de criolita da mina Pitinga (Amazonas)
J.O. Marini, E. Queiroz, B.W. Ramos (Eds.), Caracterização de Depósitos Minerais em Distritos Mineiros da Amazônia, DNPM/CTMINERAL/ADIMB, Brasília (2005), pp. 477–552

A.C. Bastos Neto, V. Pereira, L.H. Ronchi, E.F. Lima, J.C. Frantz
The Sn, Nb, Ta, F (Y, REE, Li) world class deposit and the massive cryolite deposit associated with the albite-enriched facies of the Madeira A-type granite, Pitinga mining district, Amazonas State, Brazil
Canadian Mineralogist, 47 (2010), pp. 1328–1358

A.C. Bastos Neto, V. Pereira, A.C. Pires, L. Barbanson, A. Chauvet
F-rich xenotime from the Nb–Ta–Sn Madeira world-class deposit associated with the albite-enriched granite at Pitinga (Amazonian, Brazil)
Canadian Mineralogist, 50 (2012), pp. 1453–1466

R.M.K. Borges
Greisens e epi-sienitos potássicos associados ao Granito Água Boa, Pitinga (AM): um estudo dos processos hidrotermais geradores de mineralizações estaníferas
(Doctoral thesis) Federal University of Pará, Belém, Brazil (2002) 383 pp.

R.M.K. Borges, R.N.N. Villas, K. Fuzikawa, R. Dall'Agnol, M.A. Pimenta
Phase separation, fluid mixing, and origin of the greisens and potassic episyenite associated with the Água Boa pluton, Pitinga tin province, Amazonian Craton, Brazil
Journal of South American Earth Sciences, 27 (2009), pp. 161–183

F. Chemale, R. Scheepers, P.G. Gresse, W.R. Schmus
Geochronology and sources of late Neoproterozoic to Cambrian granites of the Saldania Belt
International Journal of Earth Sciences, 100 (2011), pp. 431–444

F. Corfu, J.M. Hanchar, P.W.O. Hoskin, P. Kinny
Atlas of zircon textures
J.M. Hanchar, Hoskin (Eds.), Reviews in Mineralogy and Geochemistry, 53 (2003), pp. 469–500

H.T. Costi
Petrology of Rare Metals-, High-F-Alkaline Granites: The Example of the Albite Granite From the Pitinga Mine, Amazonas State, Brazil
(Doctoral thesis)\\ Federal University of Pará, Belém, Brazil (2000) 345 pp.

H.T. Costi, R. Dall'Agnol, C.A.V. Moura
Geology and Pb–Pb geochronology of Paleoproterozoic volcanic and granitic rocks of Pitinga Province, Amazonian Craton, Northern Brazil
International Geology Review, 42 (2000), pp. 832–849

H.T. Costi, R. Dall'Agnol, M. Pichavant, O.T. Rämo
The peralkaline tin-mineralized Madeira cryolite albite-rich granite of Pitinga, Amazonian Craton, Brazil: petrography, mineralogy and crystallization processes
Canadian Mineralogist, 47 (2010), pp. 1301–1327

W.E.K. Daoud, A. Antonietto Jr.
Geologia do granito Água Boa, Pitinga, Amazonas
Simpósio de Geologia da Amazônia, 2, Belém, 1985, Anais, 3 (1985), pp. 17–33

J.M.T.M. Ferron, A.C. Bastos Neto, S.B.A. Rolim, R. Hoff, L.V. Umann, O.R.R. Minuzzi
Reconhecimento de uma mega-estrutura no distrito mineiro de Pitinga-AM: dados preliminares a partir da aplicação de técnicas de processamento digital de imagens ETM + Landsat 7
II Simpósio de Vulcanismo, Belém, Brazil, Anais, 1 (2002), p. 14

J.M.T.M. Ferron, A.C. Bastos Neto, E.F. Lima, H.T. Costi, C. Moura, M. Prado, M. Galarza
Geologia e geocronologia Pb–Pb de rochas graníticas e vulcânicas ácidas a intermediárias Paleoproterozóicas da Província Pitinga, Craton Amazônico
Revista Brasileira de Geociências, 36 (3) (2006), pp. 499–512

J.M.T.M. Ferron, A.C. Bastos Neto, E.F. Lima, L.V.S. Nardi, H.T. Costi, R. Pierosan, M. Prado
Petrology, geochemistry, and geochronology of Paleoproterozoic volcanic and granitic rocks (1.89–1.88 Ga) of the Pitinga province, Amazonian Craton, Brazil
Journal of South American Earth Sciences, 29 (2010), pp. 483–497

R.A. Fuck, M.M. Pimentel, N. Machado, W.E.K. Daoud
Idade U–Pb do Granito Madeira, Pitinga (AM) 1993
4th Congresso Brasileiro de Geoquímica, Brasília (1993), pp. 246–249 (Extended abstract)

R.S. Issler, A.R.F. Andrade, R.M.G. Montalvão, G. Guimarães, G.G. Silva, M.I.C. Lima
Geologia da Folha SA.22. Departamento Nacional da Produção Mineral, Projeto RADAMBRASIL, Rio de Janeiro
Levantamento de Recursos Naturais, 5 (1974), pp. 7–182

S.E. Jackson, N.J. Pearsona, W.L. Griffina, E.A. Belousova
spectrometry to in situ U–Pb zircon geochronology
Chemical Geology, 211 (2004), pp. 47–69

S.L. Lenharo
Evolução magmática e modelo metalogenético dos granitos mineralizados da região de Pitinga, Amazonas, Brasil, São Paulo
(Doctoral thesis) University of São Paulo, São Paulo, Brazil (1998) 290 pp.

K.R. Ludwig
User's Manual for Isoplot/Ex version 3.00-A Geochronology Toolkit for Microsoft Excel, No. 4
Berkeley Geochronological Center Special Publication (2003) 70 pp.

P. Mandetta, J.P. Veiga Jr., J.R. Oliveira
Reconhecimento geológico ao longo do rio Pitinga, afluente do rio Uatumã
Companhia de Pesquisa de Recursos Minerais, Manaus (1974) 31 pp. (unpublished report)

R.F. Martin
A-type granites of crustal origin ultimately result from open-system fenitization-type reactions in an extensional environment
Lithos, 91 (2006), pp. 125–136

O.R.R. Minuzzi
Gênese e evolução da mineralização de criolita, pirocloro e columbita da subfácies albita granito de núcleo, mina Pitinga, Amazonas, Brasil
(Doctoral thesis) Federal University of Rio Grande do Sul, Porto Alegre, Brazil (2005) 182 pp.

O.R.R. Minuzzi, A.C. Bastos Neto, V.P. Pereira, J.A.A. Flores
O depósito criolítico maciço e o minério disseminado de criolita da mina Pitinga (Amazonas, Brasil)
Revista Brasileira de Geociências, 36 (Suppl.) (2006), pp. 104–123

R. Pierosan, E.F. Lima, L.V.S. Nardi, C.P. Campos, A.C. Bastos Neto, J.M.T.M. Ferron, M. Prado
Paleoproterozoic (~1.88 Ga) felsic volcanism of the Iricoumé Group in the Pitinga Mining District area, Amazonian Craton, Brazil: insights in ancient volcanic processes from field and petrologic data
Anais da Academia Brasileira de Ciências, 83 (2011), pp. 921–937

R. Pierosan, E.F. Lima, L.V.S. Nardi, A.C. Bastos Neto, C.P. Campos, J.M.T.M. Ferron, M. Prado
Geochemistry of palaeoproterozoic volcanic rocks of the iricoume group, Pitinga Mining District, Amazonian Craton, Brazil
International Geology Review, 53 (2011), pp. 946–976

M. Prado, J.M.T.M. Ferron, E.F. Lima, A.C. Bastos Neto, V.P. Pereira, O.R.R. Minuzzi, R. Pierosan
Caracterização petrográfica e geoquímica da parte leste do granito Europa, distrito mineiro de Pitinga, AM
Revista Pesquisas, 34 (1) (2007), pp. 77–99

J.O.S. Santos, L.A. Hartmann, H.E. Gaudette, D.I. Groves, N.J. Mcnaughton, I.R. Fletcher

A new understanding of the Amazon Craton Provinces based on integration of field mapping and U–Pb and Sm–Nd geochronology
Gondwana Research, 3 (4) (2000), pp. 453–488

J.O.S. Santos, L.A. Hartmann, N.J. McNaugthon, I.R. Fletcher
Timmin of mafic magmatism in the Tapajós Province (Brazil) and implications for the evolution of the Amazon Craton: evidence from baddeleyite and zircon U–Pb SHRIMP geochronology
Journal of South American Earth Sciences, 15 (2002), pp. 409–429

C. Schobbenhaus, A. Hope, A. Lork, A. Baumann
Idade do magmatismo Uatumã no norte do Cráton Amazônico, Escudo das Guianas (Brasil): primeiros resultados
Congresso Brasileiro de Geologia, 38, Balneário Camboriú, 2 (1994), pp. 395–397

J.S. Stacey, J.D. Kramers
Approximation of terrestrial lead isotope evolution by a two-stage model
Earth and Planetary Science Letters, 26 (1975), pp. 207–221

R. Thomas, J.D. Webster, D. Rhede, W. Seifert, K. Rickers, H.-J. Föster, W. Heinrich, P. Davidson
The transition from peraluminous to peralkaline granite melts: evidence from melt inclusions and accessory minerals
Lithos, 91 (2006), pp. 137–149

J.P. Veiga Jr., A.C.B. Nunes, A.S. Fernandes, J.E. Amaral, M.R. Pessoa, S.A.S. Cruz
Projeto Sulfetos de Uatumã
Companhia de Pesquisa de Recursos Minerais, Manaus (1979) (unpublished report)